13th IEA Heat Pump Conference
April 26-29, 2021 Jeju, Korea

# High-resolution surface plasmon resonance imaging of an evaporating droplet on the surface

Chan Ho Jeong[a], Hyung Joo Lee[a], and Seong Hyuk Lee[a,*]

[a]School of Mechanical Engineering, Chung-Ang University, 221 Heukduk-dong, Dongjak-gu, Seoul 156756, South Korea

**Abstract**

The present study aims to investigate the characteristics of evaporating thin film (ETF) in the interfacial region during evaporation. High-resolution imaging technology was used for visualization of a sessile droplet based on the surface plasmon resonance phenomena. In particular, the influence of surface wettability on the depinning behavior and the evaporation flux near the edge of a sessile droplet was examined. To resolve the singularity problem occurring at the edge of a droplet, the current study suggests a single-valued boundary limit which can be imposed at the edge, based on the experimental data. From the result, it is found that the estimated ETF distribution shows a similar order of magnitude to the profiles predicted by the Maxwell equation. There is also little influence of droplet volume on the ETF thickness and width, indicating that interfacial phenomena in the contact line region are affected mainly by wettability, not by droplet volume.

*Keywords: Evaporating thin film (ETF); Surface plasmon resonance (SPR) imaging; depinning behavior;contact line region*

## 1. Introduction

Droplet evaporation is regarded as one of commonly occurring processes in the surrounding nature and an important physical phenomenon that controls heat and mass transfer through a phase change. It can also be applied to various industrial fields such as spray cooling, direct injection engines, and heat exchangers [1]. As a matter of fact, a lot of studies have reported the dynamic behavior of droplet evaporation, related to heat transfer enhancement [2]. Using the theoretical equation based on Fick's law, the infinite flux was shown at the edge of a droplet showing singularity [3]. This singularity wouldn't be real because finite but maximum evaporation takes place in the contact line region. Cachile et al. [4] obtained the local flux distribution explicitly for the droplet with very high wettability, and Hu and Larson [3] estimated the local evaporation flux which rapidly increased at the edge of the droplet. Xie at al. [5] tried to resolve this singularity by using the molecular dynamics simulations on hydrophilic and hydrophobic surfaces, and they showed there is finite evaporation flux in the contact line. Physically, the contact line region has three regions such as adsorbed film, evaporating thin film (ETF), and bulk meniscus regions [6]. The ETF represents a liquid thin film evaporating between adsorbed film and bulk meniscus. Due to the sub-micron scale, it is very difficult to directly visualize the ETF region. Instead, most of the studies on the ETF have been carried out by theoretical and numerical manners [7].

Hence, the near-field visualization methods should be adopted for showing the ETF and examining its characteristics. As one of earlier efforts, we used the confocal microscopy for visualization of the ETF [8], successively showing micro-scale thin film emanating from the bulk droplet. The present study used the surface plasmon resonance (SPR) imaging to capture the sub-micron scale ETF because this method is capable of being of very high vertical resolution with a few tens nanometer. Indeed, we have successfully visualized the sub-micron frost layer between the frozen droplets and conducted quantitative measure of frozen layer thickness by using the surface plasmon resonance imaging microscope (SPRIM) [9]. Based on the previous study, the present study aims to visualize the ETF region of the sessile droplet on the surface and to estimate

* Corresponding author. Tel.: +82 2 820 5254; fax: +82 2 820 5254
*E-mail address:* shlee89@cau.ac.kr

the thin film thickness by using the SPR imaging. In particular, we suggested the new evaporation flux model with the measured length of the ETF region by estimating a finite boundary limit. In the following sections, the present study describes the details of experiments and the theoretical modeling, and also presents the experimental results. In the end, the results are summarized in the conclusion.

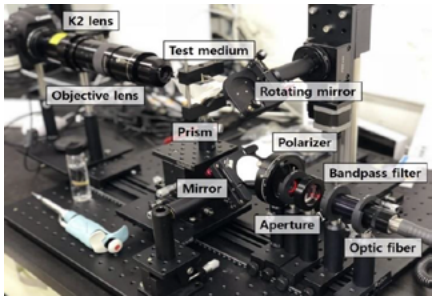



Fig. 1. Experimental setup (SPRI system).

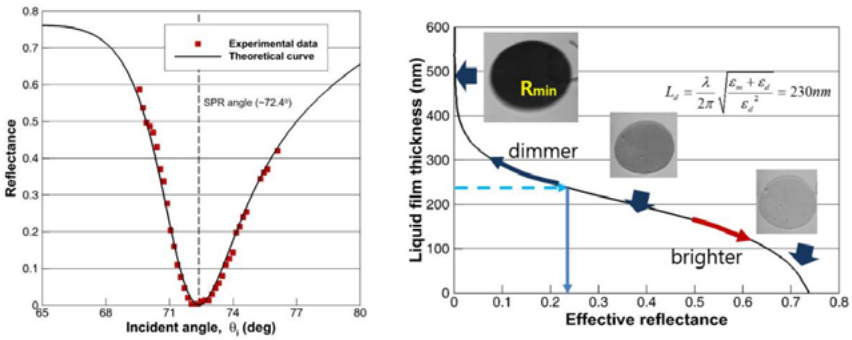



Fig. 2. a) reflectance variation with incident angle, b) liquid film thickness with respect to effective reflectance.

## 2. Experiment and modeling

To determine the flux profile along the liquid-vapor interface of the sessile droplet, most of the previous works have adopted the diffusion-limited model, assuming that the transfer rate depends on the diffusion of saturated vapor during evaporation [10]. Moreover, the evaporation flux along the liquid-vapor interface of the droplet is eventually determined by the overall shape of droplet [11]. So, we used the analogy between vapor concentration and electrostatic distribution, the evaporation flux can be expressed by [12]. We can estimate the evaporation flux along the interface by

$$J(r) = \frac{D(1-RH)c_{sat}}{R_i}\left[\frac{1}{2}\sin\theta + \sqrt{2}(\cosh\alpha + \cos\theta)^{3/2} \times \int_0^\infty \frac{\cosh\theta\tau}{\cosh\pi\tau}\tanh[(\pi-\theta)\tau]P_{-1/2+i\tau}(\cosh\alpha)\tau\, d\tau\right] \quad (1)$$

where $J$ is evaporation flux, $D$ is diffusivity of 26.1 mm$^2$/s [13], $c_{sat}$ is saturated vapor concentration of 2.32 $\times$ 10$^{-8}$ g/mm$^3$ [3], RH is relative humidity, $R_i$ is droplet contact diameter, $r$ is the radial position, $\theta$ is contact angle of the sessile droplet, and $P$ is the representation of Legendre function.

As shown in Fig. 1, the present study uses the surface plasmon resonance imaging (SPRi) system because this method has very high vertical resolution, making it possible to visualize the evaporating thin films in the contact line region. The long-distance K2 lens with 9.6× magnification was attached to CMOS camera (CANON, EOS 7D), with a pixel resolution of 680 nm. The CMOS camera captured the single-wavelength light reflected from the prism at one frame per second. The right-angle prism consists of BK7 glass (Edmund Optics), and its corresponding refractive index is 1.516 (at $\lambda$ = 632 nm). The coverslip with a 50 nm gold thin layer (Platypus Tech., Au.0500.CSS) on the 2.5 nm titanium adhesion layer was attached to the prism by using an index

matching liquid (Norland, IML150) with the same refractive index of the BK7 glass. The light irradiated from the halogen lamp (Dolan-Jenner) is converted into a single wavelength light beam through a bandpass filter (632 ± 5 nm, Edmund Optics). A collimation lens array is installed to convert the diverging light beam into a parallel light beam.

As shown in Fig. 2(a), the measure reflectance shows very good agreement with the theoretical solutions from Maxwell equation and thin film optics theory. The surface plasmon is representing the energy carrier being charged, and the evanescent wave propagates along the interface between two dissimilar layers. For water phase, the incident angle of 72.4 degree is called SPR angle at which the minimum reflectance occurs, indicating that mostly absorbed energy is converted into evanescent waves. At this condition, SPRi system enables to capture the images with different contrast levels between zero and 256 based on 8 bits. Figure 2(b) shows the change of liquid film thickness estimated theoretically with the reflectance. This figure indicates that the liquid film thickness can be directly matched with the corresponding reflectance. It means once the reflectance is measured, the liquid film thickness can be estimated through the relationship shown in Fig. 2(b). As the captured image gets dimmer, the liquid film gets thicker, vice versa. Interestingly, we can get 500 nm thickness with very high vertical resolution, being of approximately 1.8 nm based on our facility. We used Kretschmann's configuration for SPR imaging with the white light illuminated from an LED light source which was passed through the optic arrays. A single wavelength light (632 ± 5 nm) and p-polarized ray was used for visualization. The ray is guided onto the prism by using the rotatable mirror with a specific incident angle (72.4°). The gold coated thin film is attached to the prism.

Once the liquid film thickness is measured with SPRi system, the evaporation flux at the droplet edge can be modeled as illustrated in Fig. 3. Geometrically, the inflection point on the droplet interface can be estimated by using the measured film thickness. Hence, we finally determine the width of evaporating thin film as shown in Fig. 3. Here, we suggest a new parameter called the averaged evaporation flux (AEF), as shown in Eq. (2). Using this equation, we can get the averaged value over the contact line region by mass conservation, showing the finite (not infinite value) evaporation flux limit can be obtained.

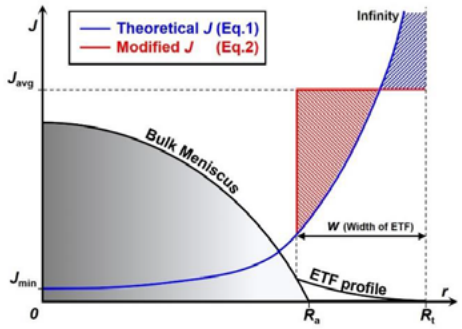



Fig. 3. Concept of the averaged evaporation flux modelling based on the measured width.

$$J_{avg} = \left( \int_{R_t - w}^{R_t} J \, dr \right) / w \tag{2}$$

where $R_t$ is total contact radius of droplet considering ETF region, and $R_a$ is apparent contact radius of spherical cap, $w$ means the width of ETF, and $J_{avg}$ denotes the AEF in the ETF which is treated as the boundary limit mathematically. For closing this equation, it is necessary to get the experimental measures of width and thickness of ETF. Those measures were obtained by the SPRIM system used in the present study.

## 3. Results and discussion

Figure 4 shows the measured ETF profiles. The measurements were made five times for getting the averaged values with relative errors. A convex shape was observed consistently at different droplet volumes. Indeed, the shape of ETF has been explained by the force balance along the triple lines according to Young-Laplace model and kinetic theory. As shown in Fig. 4, we can see that a slight change in liquid film thickness is observed, indicating that the shape of ETF does not change with time by interacting with the bulk droplet region.

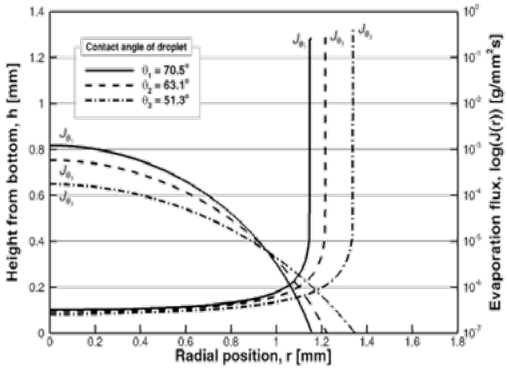
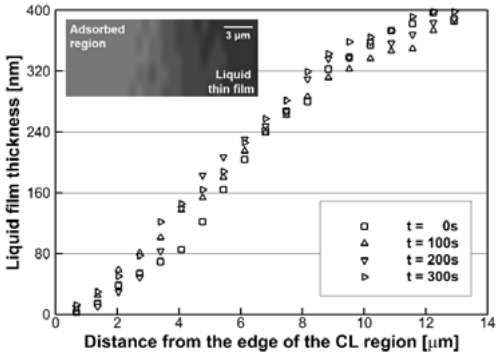



Fig. 4. The measured liquid film thickness with respect to time.

Based on this result, we can estimate the averaged evaporation flux as shown in Fig. 5. For validation, the evaporation flux at the apex of droplet showed being of the same value compared with the data from Hu and Larson [3]. The maximum evaporation flux was estimated to be 0.2547 g/mm$^2$·s, 0.2486 g/mm$^2$·s, and 0.2486 g/mm$^2$·s for the droplet volume of 2 μl, 4 μl, and 6 μl, respectively. It shows that the averaged evaporation flux predicted in the ETF becomes getting higher for smaller drops. That is, the smaller the droplet volume, the greater the absolute amount of evaporation flux in the ETF region. It means the portion of evaporation flux in the ETF region cannot be ignored for smaller droplet.

Fig. 5. Real-scale droplet meniscus and scaled evaporation flux considering ETF region with respect to drop volume at the initial stage.




## 4. Conclusions

This study reported that there exists the evaporating thin film clearly in the contact line region by the SPR imaging method. We also suggested the new approach to estimate the averaged evaporation flux. The following conclusions were drawn.

1) We observed the existence of an ETF and measured its profile in the contact line region. It indicates that the current SPR system can successfully measure the submicron liquid film thickness.
2) The present study investigated the effect of droplet volume on the ETF profile, but it was negligible. Although the droplet volume increased, the profile of ETF remains consistent shape in the contact line region because it was affected by the interfacial forces with the bulk region. Also, we estimated the averaged evaporation flux in the contact line by using the measured data. It could be used to overcome the singularity problem of the diffusion-limited model. It was shown that the contribution of ETF to evaporation was dominant as the droplet volume decreased. It is also noted that the smaller droplet was

significantly affected by the ETF which cause the higher mass transfer.

**Acknowledgements**

This work was supported by a National Research Foundation of Korea (NRF) grant funded by the Korea government (MSIT) (No. 2017R1A2B2006943). Also, this research was partially supported by the development of human resources for design specialists in applications of functional materials (Brain Korea (BK) 21).

**References**

[1] D. Mampallil and H. B. Eral, A review on suppression and utilization of the coffee-ring effect, Advances in Colloid and Interface Science, 252 (2018) 38-54.
[2] R. D. Deegan, O. Bakajin, T. F. Dupont, G. Huber, S. R. Nagel, and T. A. Witten, Contact line deposits in an evaporating drop, Physical Review E, 62 (2000) 756-65.
[3] H. Hu and R. G. Larson, Evaporation of a sessile droplet on a substrate, Journal of Physical Chemistry B, 106 (6) (2002) 1334-1344.
[4] M. Cachile, O. Benichou, C. Poulard, and A. M. Cazabat, Evaporating droplets, Langmuir, 18 (2002) 8070-8078.
[5] C. Xie, G. Liu, and M. Wang, Evaporation flux distribution of drops on a hydrophilic or hydrophobic flat surface by molecular simulations, Langmuir, 32 (2016) 8255-8264.
[6] V. P. Carey, Liquid Vapor Phase Change Phenomena. Taylor & Francis, (2007).
[7] M. Potash Jr and P. Wayner Jr, Evaporation from a two-dimensional extended meniscus, International Journal of Heat and Mass Transfer, 15 (10) (1972) 1851-1863.
[8] D. H. Shin, J. S. Allen, C. K. Choi, and S. H. Lee, Visualization of an evaporating thin layer during the evaporation of a nanofluid droplet, Langmuir, 31 (4) (2015) 1237-1241.
[9] C. H. Jeong, D. H. Shin, V. Konduru, J. S. Allen, C. K. Choi, and S. H. Lee, Quantitative measurements of nanoscale thin frost layers using surface plasmon resonance imaging, International Journal of Heat and Mass Transfer, 124 (2018) 83-89.
[10] Y. O. Popov, Evaporative deposition patterns: spatial dimensions of the deposit, Physical Review E, 71 (2005) 036313.
[11] J. M. Stauber, S.K. Wilson, and B.R. Duffy, Evaporation of droplets on strongly hydrophobic substrates, Langmuir, 31 (2015) 3653-3660.
[12] N. N. Lebedev, Special functions and their application, Prentice-Hall: Englewood Cliffs, New Jersey, 1965.
[13] R. C. Weast and M. J. Astle, CRC handbook of Chemistry and Physics, 62nd ed.; CRC Press: Boca Raton, FL, 1981-1982.